SIAM Review
Vol. 61, No. 1, pp. 92–118

Multistate Dynamical Processes on Networks: Analysis through Degree-Based Approximation Frameworks*

Peter G. Fennell†
James P. Gleeson‡

Abstract. Multistate dynamical processes on networks, where nodes can occupy one of a multitude of discrete states, are gaining widespread use because of their ability to recreate realistic, complex behavior that cannot be adequately captured by simpler binary-state models. In epidemiology, multistate models are employed to predict the evolution of real epidemics, while multistate models are used in the social sciences to study diverse opinions and complex phenomena such as segregation. In this paper, we introduce generalized approximation frameworks for the study and analysis of multistate dynamical processes on networks. These frameworks are degree-based, allowing for the analysis of the effect of network connectivity structures on dynamical processes. We illustrate the utility of our approach with the analysis of two specific dynamical processes from the epidemiological and physical sciences. The approximation frameworks that we develop, along with open-source numerical solvers, provide a unifying framework and a valuable suite of tools for the interdisciplinary study of multistate dynamical processes on networks.

Key words. complex systems, network science, dynamical systems

AMS subject classifications. 60J27, 37N25, 05C82, 34B45

DOI. 10.1137/16M1109345

1. Introduction.

Networks are ubiquitous. From social networks to ecological networks, and from human contact networks to transportation networks to the World Wide Web, the existence of groups of units that are interconnected in some manner is common in our modern-day world [53]. When modeling dynamical processes on networks [4, 57], the most minimally complex models are those with binary state-spaces, i.e., models where, at each moment of time, a node can occupy either of two binary states [27, 45]. Nodes can change from one state to the other, and do so probabilistically with transition rates that depend on various local and global factors. Binary-state models have been applied to model many phenomena, with examples including the spread of computer viruses though the internet [38], global cascades in complex systems [71], and the diffusion of opinions or sentiment through social networks [5].

*Received by the editors December 27, 2016; accepted for publication (in revised form) April 6, 2018; published electronically February 7, 2019.
http://www.siam.org/journals/sirev/61-1/M110934.html
Funding: This work was supported by Science Foundation Ireland, grants 11/PI/1026 and 16/IA/4470, and the James S. McDonnell Foundation.

†Information Sciences Institute, University of Southern California, Marina del Rey, CA 90292 (pfennell@isi.edu).
‡MACSI, Department of Mathematics and Statistics, University of Limerick, Ireland (james.gleeson@ul.ie).

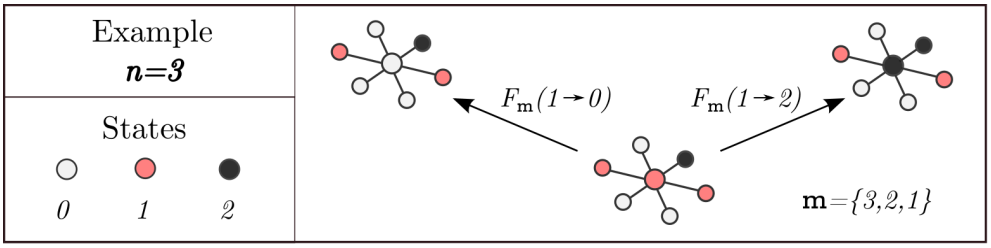

Fig. 1 *Schematic of a multistate dynamical process. In this example, nodes can be in one of three states (labeled* 0*,* 1*, or* 2*). Nodes change from their current state i to a different state j at a rate $F_{\mathbf{m}}(i \to j)$ that depends both on the state i of the node and and the states of its neighbors, where the vector $\mathbf{m} = \{m_0, \ldots, m_{n-1}\}$ encodes the number of neighbors in each of the n states.*

However, many natural phenomena cannot be adequately modeled with a simple binary state-space and extensions of the modeling framework to multiple states are required. Examples abound in the field of epidemiology, where multistate models are used to model and predict the evolution of real epidemics such as the recent Ebola outbreak in West Africa [28, 44]. Such models include various node states associated with the disease (such as susceptible, infectious, exposed) as well as other states associated to control and/or other actions (vaccinated, hospitalized, etc.) [34], and form the basis for computational platforms used to predict and develop control strategies for epidemics [3].

Despite the growing importance of multistate modeling, there exists no unifying theoretical framework to enable the analysis of how network structure affects the evolution of multistate dynamical processes. While specific frameworks have been developed in certain areas, such as for rumor spreading [16] and the dynamics of interacting diseases [59], a fully general approach that covers the whole class of multistate dynamical processes is still lacking. The purpose of this paper is to bridge that gap.

In this work, we consider the general class of continuous-time multistate dynamical processes (on undirected networks) that can be represented by rate functions $F_{\mathbf{m}}(i \to j)$, where $F_{\mathbf{m}}(i \to j)$ denotes the rate at which a node in state i changes to state j as a function of the number of its neighbors in each of the n multiple states of the dynamics (see Figure 1). This latter information is encoded in the vector $\mathbf{m} = \{m_0, \ldots, m_{n-1}\}$, where m_l is the number of neighbors of a node in state l. For a more compact representation, the rate functions can be combined into a rate function matrix $\mathbf{F}_{\mathbf{m}}$, where $(\mathbf{F}_{\mathbf{m}})_{ij} = F_{\mathbf{m}}(i \to j)$. A very wide range of multistate dynamical process models from the literature can be represented in this form, and in section 2 we give a brief review of such literature to illustrate the generality of our approach.

Using this representation, we develop degree-based approximation frameworks for the analysis of multistate dynamics on uncorrelated networks, with a focus on the effects of the network degree distribution. We develop three such frameworks with varying levels of approximation, namely, the mean-field, pair approximation, and approximate master equation frameworks [27, 53]. Furthermore, we develop software for the efficient numerical solution of these systems of differential equations, allowing for detailed analysis in the cases where the equations are not analytically tractable. While our methods are presented in a very general manner, in section 4 we examine in

detail two multistate dynamical processes specified by different rate matrix functions $\mathbf{F_m}$. Our analysis illustrates how our approach can give a deep understanding of multistate dynamical processes on a network and an appreciation for the various levels of accuracy that are required for different dynamical systems.

The paper is laid out as follows. In section 2, we review multistate dynamical process models from the literature. The general approximation frameworks are developed in section 3, while two specific multistate dynamical processes are examined in section 4. We conclude in section 5.

2. Multistate Models of Dynamical Processes. Dynamical processes in which nodes can be in one of several (more than two) discrete states have found diverse applications in a range of disciplines. In this section we provide a nonexhaustive review of relevant literature and conclude by showing how all the examples can be represented as members of a common mathematical class.

Multistate dynamical processes are prominent in the field of epidemiology, where compartmental models are widely used to model the progression of diseases through a population. The simplest epidemiological compartmental models are the susceptible-infected (SI), susceptible-infected-susceptible (SIS), and susceptible-infected-recovered (SIR) models [39], but these models are known to have limited utility in modeling real epidemics [55]. Instead, more complex multistate compartmental models are used to model and forecast real epidemics. For example, the SEIR model and its extended variants, which include an "exposed" compartment where individuals have contracted the disease but are not yet infectious, are commonly used to predict the evolution of real epidemics such as Ebola [1, 28, 43, 44] and SARS [54, 64]. The SIRS model, where recovered nodes can again become susceptible to infection after an appropriate immunity period, is used as a model for influenza that can capture the seasonal oscillations of the disease [18, 35]. In fact, multitudes of other states such as *vaccinated* [62], *maternally immune* [34], and *quarantined* [33] can be included depending on the problem being modeled; comprehensive overviews of such multi-compartmental models can be found in [2, 34]. Note that, in general, the analysis of such models assumes mean-field or homogeneous-mixing assumptions, where every node can make contact with every other node [1, 2, 28, 34, 39, 44, 62]; however, these assumptions are very often too simple for real populations, which have highly complex network structures.

It is important to understand the dynamics of multistate epidemic processes—and their interplay with the network on which they spread—in order to gain insights for the prediction and control of real diseases. One particularly important feature of the dynamics is the so-called *epidemic threshold*, a critical point in the dynamics which separates the equilibrium condition of a disease-free network (where no node is infected) from the sustained endemic state.[1] Recently, certain authors have devised generalized descriptions of multistate epidemic processes and analyzed their behavior and epidemic thresholds on complex networks; such works include those of Lin et al. [46], Guo, Li, and Shuai [31], and the $S^*I^2V^*$ model of Prakash et al. [58]. Also noteworthy is the work of Masuda and Konno [48] who, despite not presenting a generalized model, examine the epidemic thresholds of a wide variety of multistate epidemic processes using degree-based mean-field approaches [55]. Note at this point that different theoretical approaches can lead to differing predictions of the epidemic

[1] Strictly speaking, this definition of the epidemic threshold only applies to the idealized case of networks with an infinite number of nodes. In finite networks, the disease will always die out eventually; in this case, the epidemic threshold has been defined [17] such that below the threshold the disease dies out exponentially fast, while above the threshold it dies out logarithmically slowly.

threshold, and thus extensive numerical simulation can be essential to gauging the accuracy or limitations of such theories [49, 22].

Recently, much focus has shifted to the area of interacting diseases, where multiple diseases coexist in a population and where each disease can affect the progression of the others [12, 32, 59]. This work has been motivated by dependencies between real diseases, such as the increased rate of tuberculosis progression in individuals who are infected with HIV [14]. Interacting disease dynamics are naturally expressed in a multistate setting, where the state of each node encodes whether it is susceptible, infected, etc., for each of the coexisting diseases. This construction also applies to general multiply-interacting dynamical processes such as, for example, the interplay between the spread of a disease and the spread of awareness or information about the disease [29].

Because epidemiological models describe the diffusion of contagions through a network, they have also been widely employed to model diffusions in the social and life sciences [7]. The Bass model for the diffusion of innovations is a well-known variant of the SI model that includes external influences, and multistate extensions such as the four-state model of Mellor et al. [50] have been proposed to address limitations that can arise because of the simplicity of the original Bass model. Similarly, multistate contagion models have been used to realistically model a variety of social phenomena, such as Xiong et al.'s four-state model of information spread [72] and the four-state fanaticism model of Castillo-Chavez and Song [9] and Stauffer and Sahimi [66]. The general multistage model of Krapivsky and Redner [40] models the spread of innovations and fads, where the multiple stages represent the social reinforcement required before individuals eventually adopt a behavior, while de Arruda et al. [16] developed a unifying approach for rumor and disease spreading. Very recently, Kyriakopoulos et al. [42] examined approximation methods for multistate contact processes and developed an aggregation scheme to cluster together nodes with similar dynamical behavior, thus reducing the number of equations to be solved.

Epidemiological models are not sufficient, however, to capture all kinds of human interaction behavior, and several other classes of model exist. One of the most widely studied models of social dynamics in the statistical physics literature is the voter model [7, 65], which models the adoption of opinions by members of a population through the mechanism of imitation. In its original binary-state form, the voter model eventually leads to consensus within a finite population, where every individual eventually adopts the same opinion [45]. However, real social dynamics often display richer phenomena, such as social segregation [60], and so multistate variations of the voter model have been introduced that can account for such complex behaviors. The Leftists, Centrists, and Rightists in the model of Vazquez et al. [67, 68] produce spatially heterogeneous equilibrium states where clusters of Leftists coexist alongside clusters of Rightists. Other multistate voter models produce sustained metastable states of spatial heterogeneity before relaxing to consensus: examples of such models include the four-state confident voting model of Volovik and Redner [70], the noise reduced voter model of [15], and the three-state AB model of Castelló, Baronchelli, and Loreto [8]. Similarly, in some multistate voter models consensus is never reached, such as the model of Volovik, Mobilia, and Redner [69], which includes noise terms that allow for both the suppression or the equalization of opinions. Another multistate model that is well studied in the statistical physics literature is the Potts model, a multistate extension of the Ising model which, although originally formulated as a model of ferromagnets, has been used to model cellular dynamics and opinion dynamics [7].

Finally, we discuss threshold models, models of diffusion that differ fundamentally from the voter and epidemiological type models [71]. These models describe "complex contagions," where numerous exposures to an innovation are required before an agent adopts [10]. Specifically, individual nodes in a threshold model will only adopt a behavior if the fraction of their neighbors who have previously adopted is above a certain threshold. Traditional binary-state threshold models have been extensively studied, and recently multistate threshold models been proposed. Melnik et al. [51] introduced a "progressive" three-state model, where agents have two thresholds, while Kuhlman and Mortviet [41] extended this formalism, allowing an arbitrary number of states and transitions from each state to every other state. A similar nonlinear model is the multistate majority rule model [13], where every node has a multitude of opinions and nodes change their opinion depending on the majority opinion of groups to which they belong.

The models discussed above, although stemming from a diverse range of disciplines with different motivating questions, can all be represented as members of a common mathematical class. In each model, nodes are in one of a discrete number n of states, which we can generically denote as $\{0, 1, \ldots, n-1\}$ (see Figure 1). Nodes can dynamically change from their current state to another state and do so at a stochastic rate $F_{\mathbf{m}}(i \to j)$ that depends on both their own state and on the states of their neighbors, encoded in the vector $\mathbf{m} = \{m_0, m_1, \ldots, m_{n-1}\}$, where m_l is the number of neighbors of a node in state l. We note the important fact that the rate functions that we study here are independent of time t; the dynamical processes that we study here are therefore memoryless or Markovian.

3. Approximation Frameworks. In this section we develop approximation frameworks for the analysis of multistate stochastic dynamical processes, by generalizing the methods for binary-state dynamics of [26, 27]. We consider undirected, unweighted networks with a given degree distribution p_k, where p_k is the probability that a randomly chosen node in the network has degree k. We assume that the number N of nodes in the network is very large (taking the $N \to \infty$ limit) and that the networks are maximally random subject to the constraint of the degree distribution, e.g., networks drawn from the configuration model ensemble [53]. Such networks are useful in studying how network connectivity (i.e., the distribution of degrees) affects dynamical processes taking place on networks; however, they do not possess degree-degree correlations, transitivity, or other structural properties that are characteristic of real-world networks [53].

Each node in the network can be in one of n states and nodes change state from their current state i to another state j at a rate $F_{\mathbf{m}}(i \to j)$ (which can be zero in the case that a transition $i \to j$ is not possible). The rate functions $F_{\mathbf{m}}(i \to j)$, for $0 \leq i, j \leq n-1$ (or, equivalently, the rate matrix function $\mathbf{F}_{\mathbf{m}}$), fully define the continuous-time Markovian dynamical process. In section 3.1 we present the approximate master equations (AMEs), followed by the pair approximation (PA) framework in section 3.2 and finally the mean-field (MF) framework in section 3.3. The reason for this order is that the PA equations can be deduced from the AMEs by making appropriate simplifying assumptions, and similarly the MF equations can be deduced from the PA equations under further assumptions.

3.1. Approximate Master Equation. The approximate master equation (AME) is a theoretical framework for studying dynamical processes that has been shown to reproduce a range of binary-state dynamics to a high level of accuracy [21, 26, 27, 47]. We define as $x^i_{k,\mathbf{m}}(t)$ the variables of the multistate AME, where $x^i_{k,\mathbf{m}}(t)$ is the

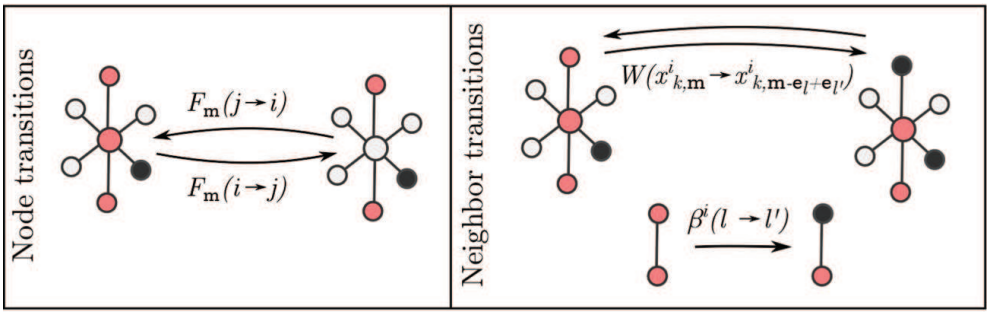

Fig. 2 *Transitions between classes in the AME formalism. Nodes change from one class to another because either they change state (left) or one of their neighbors changes state (right). The node transitions are fully specified by the rate functions $F_{\mathbf{m}}(i \to j)$. The neighbor transition rates $W(x^i_{k,\mathbf{m}} \to x^i_{k,\mathbf{m}-\mathbf{e}_l+\mathbf{e}_{l'}})$ are approximated by link transition rates $\beta^i(l \to l')$ as given by* (4) *and* (5).

expected fraction of k-degree nodes in the network that are in state i and have $\mathbf{m}$ neighbors in each of the various states at time t. These variables are defined for all states $0 \le i \le n-1$, for all possible degree classes $k_{\min} \le k \le k_{\max}$, and—for each degree class k—for all values of $\mathbf{m}$ such that $\sum_{l=0}^{n-1} m_l = k$. From these variables, one can obtain various macroscopic quantities related to the evolution of the dynamics on the network, such as the expected fraction $\rho^i(t)$ of the population in state i at time t:

$$\rho^i(t) = \Big\langle \sum_{|\mathbf{m}|=k} x^i_{k,\mathbf{m}}(t) \Big\rangle_k. \tag{1}$$

Here $\sum_{|\mathbf{m}|=k}$ is the sum over all values of $\mathbf{m}$ such that $\sum_{l=0}^{n-1} m_l = k$ and $\langle\cdot\rangle_k = \sum_{k=0}^{\infty} p_k \cdot$ symbolizes averaging over the degree distribution p_k.

To derive the evolution equations that describe how the variables $x^i_{k,\mathbf{m}}(t)$ change over time, we consider all ways in which nodes can leave and enter the $x^i_{k,\mathbf{m}}$ class. These changes are illustrated in the schematic of Figure 2. On one hand, nodes in the $x^i_{k,\mathbf{m}}$ class will *leave* that class because either the node itself changes state (a "node transition") or because one of its neighbors changes state, and thus the vector $\mathbf{m}$ changes (a "neighbor transition"). In an (infinitesimally small) time interval Δt, a $x^i_{k,\mathbf{m}}$ node will change from state i to state j with probability $F_{\mathbf{m}}(i \to j)\Delta t$, and so the expected fraction of nodes in the $x^i_{k,\mathbf{m}}$ class that change to state j is $x^i_{k,\mathbf{m}}(t)F_{\mathbf{m}}(i \to j)\Delta t$. Accounting for all states $j \ne i$, the expected fraction of nodes that leave the $x^i_{k,\mathbf{m}}$ class because they themselves change state from state i is

$$\sum_{j \ne i} x^i_{k,\mathbf{m}}(t) F_{\mathbf{m}}(i \to j)\Delta t. \tag{2}$$

In addition, nodes can leave the $x^i_{k,\mathbf{m}}$ class because their neighbors change state. The probability that a neighbor of such a node that is currently in state l changes to state l' in the infinitesimal time interval Δt is given by

$$W(x^i_{k,\mathbf{m}} \to x^i_{k,\mathbf{m}-\mathbf{e}_l+\mathbf{e}_{l'}})\Delta t, \tag{3}$$

where $W(x^i_{k,\mathbf{m}} \to x^i_{k,\mathbf{m}-\mathbf{e}_l+\mathbf{e}_{l'}})$ is a neighbor transition rate and $\mathbf{e}_l$ (resp., $\mathbf{e}_{l'}$) is the standard unit basis vector which is zero everywhere except at position l (resp., l') (and

so $\mathbf{m} - \mathbf{e_l} + \mathbf{e_{l'}} = \{\dots, m_l - 1, \dots, m_{l'} + 1, \dots\}$). It is in these neighbor transition rates that we make the AME approximation in order to create a closed system of equations. This approximation is the assumption that the transition rate of a given neighbor of a node is independent of the states of all other neighbors of the node. Thus, the rate at which a neighbor of a state i node will change from state l to state l' is assumed to be equal to the rate at which a link of type (i)–(l) changes to one of type (i)–(l'), averaged over the whole network (see Figure 2). We denote this link transition rate as $\beta^i(l \to l')$, and thus we have that the neighbor transition rate of (3) is approximated as

$$W(x^i_{k,\mathbf{m}} \to x^i_{k,\mathbf{m}-\mathbf{e_l}+\mathbf{e_{l'}}}) = m_l \beta^i(l \to l'). \tag{4}$$

The link transition rate $\beta^i(l \to l')$ is formulated by calculating a global average over the whole network, as follows. The expected number of links of type (i)–(l) in the network at time t is $N\langle \sum_{|\mathbf{m}|=k} m_i x^l_{\mathbf{m}}(t)\rangle_k$, and the expected number of these (i)–(l) links that change to (i)–(l') in the infinitesimal time interval Δt is $N\langle \sum_{|\mathbf{m}|=k} m_i x^l_{\mathbf{m}}(t) F_{\mathbf{m}}(l \to l')\Delta t\rangle_k$. Then the probability $\beta^i(l \to l')\Delta t$ that a link of type (i)–(l) changes to a link of type (i)–(l') is the ratio of these two quantities and so $\beta^i(l \to l')$ is given by

$$\beta^i(l \to l') = \frac{\langle \sum_{|\mathbf{m}|=k} m_i x^l_{k,\mathbf{m}}(t) F_{\mathbf{m}}(l \to l')\rangle_k}{\langle \sum_{|\mathbf{m}|=k} m_i x^l_{k,\mathbf{m}}(t)\rangle_k}. \tag{5}$$

Accounting for each possible transition $l \to l'$ and each of the neighbors of a node in the $x^i_{k,\mathbf{m}}$ class gives the expected fraction of nodes that leave the class during the Δt time interval because their neighbors change state:

$$\sum_{l=0}^{n-1} \sum_{l' \neq l} x^i_{k,\mathbf{m}}(t) m_l \beta^i(l \to l')\Delta t. \tag{6}$$

On the other hand, nodes in a different class will *enter* the $x^i_{k,\mathbf{m}}$ class because either their state changes to i or the state of one of their neighbors changes. A node in the $x^j_{k,\mathbf{m}}$ class will enter the $x^i_{k,\mathbf{m}}$ class if its state changes from j to i; this occurs with probability $F_{\mathbf{m}}(j \to i)\Delta t$, and if we consider all classes $j \neq i$, then the expected fraction of nodes that enter the $x^i_{k,\mathbf{m}}$ class because they change state to i is given by

$$\sum_{j \neq i} x^j_{k,\mathbf{m}}(t) F_{\mathbf{m}}(j \to i)\Delta t. \tag{7}$$

In terms of neighbor transitions, a node in the $x^i_{k,\mathbf{m}-\mathbf{e_l}+\mathbf{e_{l'}}}$ class can enter the $x^i_{k,\mathbf{m}}$ class if one of its neighbors in state l' changes to state l. This will occur with probability $(m_{l'}+1)\beta^i(l' \to l)\Delta t$, where $\beta^i(l' \to l)$ is defined as in (5), and so the expected fraction of nodes that enter the $x^i_{k,\mathbf{m}}$ class during a Δt time interval because of a neighbor changing state is

$$\sum_{l=0}^{n-1} \sum_{l' \neq l} x^i_{k,\mathbf{m}-\mathbf{e_l}+\mathbf{e_{l'}}}(t)(m_{l'}+1)\beta^i(l' \to l)\Delta t. \tag{8}$$

Thus, we have quantified all ways in which the size of the $x^i_{k,\mathbf{m}}(t)$ class can change in an infinitesimally small time interval Δt. (Note that in continuous-time Markov

processes at most one transition can occur in a sufficiently small time interval; multiple transitions occur with probabilities that are of order $(\Delta t)^2$ as $\Delta t \to 0$, and are therefore negligible when we derive the differential equations below.)

The value $x^i_{k,\mathbf{m}}(t+\Delta t)$ at the end of the Δt time interval is given by

$$x^i_{k,\mathbf{m}}(t+\Delta t) = x^i_{k,\mathbf{m}}(t) - \text{leave} + \text{enter}, \tag{9}$$

where the *leave* term of (9) is comprised of the changes given by (2) and (6) and the *enter* term is comprised of the changes given by (7) and (8). Finally, if we divide (9) by Δt, and take the limit $\Delta t \to 0$, we arrive at the evolution equation for $x^i_{k,\mathbf{m}}(t)$:

$$\begin{aligned}\frac{d}{dt}x^i_{k,\mathbf{m}} = &-\sum_{j\neq i} F_{\mathbf{m}}(i\to j)x^i_{k,\mathbf{m}} + \sum_{j\neq i} F_{\mathbf{m}}(j\to i)x^j_{k,\mathbf{m}} \\ &- \sum_{l=0}^{n-1}\sum_{l'\neq l} m_l\beta^i(l\to l')x^i_{k,\mathbf{m}} + \sum_{l=0}^{n-1}\sum_{l'\neq l}(m_{l'}+1)\beta^i(l'\to l)x^i_{k,\mathbf{m}-\mathbf{e}_l+\mathbf{e}_{l'}}.\end{aligned} \tag{10}$$

Equation (10), for $0 \le i \le n-1$ and for all values of $\mathbf{m}$ and all degree classes $k_{\min} \le k \le k_{\max}$, forms a closed set of equations that describe the evolution of the system from known initial conditions $x^i_{k,\mathbf{m}}(0)$. The number of equations in this system can be calculated by considering all possible combinations of $\mathbf{m}$ for a particular value of k. Such $\mathbf{m}$ variables must satisfy $\sum_{l=0}^{n} m_l = k$. This combinatorial problem can be directly mapped to an urn problem, where there are n different colored balls in an urn and one must draw k balls from the urn *with* replacement [19]. The number of different possible draws here is $\binom{k+n-1}{k}$, and if we consider all values of i and k, then the size of the AME system is

$$n\sum_{k=k_{\min}}^{k_{\max}}\binom{n+k-1}{k}. \tag{11}$$

Equation (11) scales superlinearly with both m and the maximum degree $k_{\max}$ of the degree distribution. In many cases, this system size can prove too large to allow for any meaningful analysis, and so in subsequent sections we define simpler systems, at the cost of further approximation.

3.2. Pair Approximation Framework. The AME makes the assumption that the transition rate of a neighbor of a given node is independent of the states of all other neighbors of the node. The pair approximation (PA) goes a step further by assuming that the *state* of a neighbor of a given node is independent of the states of all other neighbors of the node. Dynamical correlations between a node and each individual nearest neighbor are considered, but the states of the neighbors of the node are assumed to be independent. We define as $x^i_k(t)$ and $q^{i\to j}_k(t)$ the variables of the multistate PA, where $x^i_k(t)$ is the fraction of k-degree nodes in state i at time t and $q^{i\to j}_k(t)$ is the probability at time t that a randomly chosen link emanating from a k-degree node in state i leads to a node in state j. Under the PA assumption that the states of the neighbors of a node are independent, the probability of having $\mathbf{m}$ neighbors in each of the various states is multinomially distributed. If we denote by $\text{Mult}_{k,i}(\mathbf{m})$ the probability that a k-degree node in state i has $\mathbf{m}$ neighbors in the various different states at time t, then $\text{Mult}_{k,i}(\mathbf{m})$ is given by

$$\text{Mult}_{k,i}(\mathbf{m}) = \frac{k!}{m_0!\dots m_{n-1}!}(q^{i\to 0}_k(t))^{m_0}\dots(q^{i\to m-1}_k(t))^{m_{n-1}}. \tag{12}$$

By making the PA independence assumption, the AME variables $x^i_{k,\mathbf{m}}(t)$ reduce to

$$x^i_{k,\mathbf{m}}(t) = x^i_k(t)\mathrm{Mult}_{k,i}(\mathbf{m}). \tag{13}$$

Note that the sum of the multinomial probabilities of (12) over all values of $\mathbf{m}$ with $|\mathbf{m}| = k$ is 1, and performing this sum on both sides of (13) gives a direct relationship between the PA variable $x^i_k(t)$ and the AME variables $x^i_{k,\mathbf{m}}(t)$:

$$x^i_k(t) = \sum_{|\mathbf{m}|=k} x^i_{k,\mathbf{m}}(t). \tag{14}$$

By differentiating both sides of (14) with respect to time, and inserting the PA ansatz of (13) into the right hand side of the evolution equation (10) for $x^i_{k,\mathbf{m}}$, we arrive at the PA evolution equation for $x^i_k(t)$:

$$\begin{aligned}\frac{d}{dt}x^i_k = &-\sum_{j\neq i} x^i_k \sum_{|\mathbf{m}|=k} F_{\mathbf{m}}(i\to j)\mathrm{Mult}_{k,i}(\mathbf{m}) \\ &+\sum_{j\neq i} x^j_k \sum_{|\mathbf{m}|=k} F_{\mathbf{m}}(j\to i)\mathrm{Mult}_{k,j}(\mathbf{m}).\end{aligned} \tag{15}$$

The evolution equations for the other variables of the PA system, $q^{i\to j}_k(t)$, are constructed from the AMEs in the following manner. In the AME, the expected number of links of type $(i)_k$–(j) at time t (i.e., links emanating from k-degree nodes in state i that lead to a node in state j) is $N\sum_{|\mathbf{m}|=k} m_j x^i_{k,\mathbf{m}}(t)$. By multiplying the PA ansatz of (13) by Nm_j, summing over all values with $|\mathbf{m}| = k$, and using the fact that $\sum_{|\mathbf{m}|=k} m_j\mathrm{Mult}_{k,i}(\mathbf{m}) = kq^{i\to j}_k(t)$, we obtain

$$N\sum_{|\mathbf{m}|=k} m_j x^i_{k,\mathbf{m}}(t) = Nx^i_k(t)kq^{i\to j}_k(t). \tag{16}$$

Differentiating both sides of (16) with respect to time, cancelling the common factor N, and rearranging gives

$$\frac{d}{dt}q^{i\to j}_k = -\frac{1}{x^i_k}\left(\frac{dx^i_k}{dt}q^{i\to j}_k - \sum_{|\mathbf{m}|=k}\frac{m_j}{k}\frac{dx^i_{k,\mathbf{m}}}{dt}\right). \tag{17}$$

Inserting into (17) the expressions for dx^i_k/dt and $dx^i_{k,\mathbf{m}}/dt$ from (15) and (10), respectively, and using the PA ansatz of (13), gives the evolution equation for $q^{i\to j}_k(t)$:

$$\begin{aligned}\frac{d}{dt}q^{i\to j}_k = &\\ \sum_{|\mathbf{m}|=k}\left(q^{i\to j}_k - \frac{m_j}{k}\right)&\left(\sum_{l\neq i} F_{\mathbf{m}}(i\to l)\mathrm{Mult}_{k,i}(\mathbf{m}) - \frac{x^l_k}{x^i_k}F_{\mathbf{m}}(l\to i)\mathrm{Mult}_{k,l}(\mathbf{m})\right) \\ &+\sum_{l=0}^{n-1}\left(q^{i\to l}_k\beta^i(l\to j) - q^{i\to j}_k\beta^i(j\to l)\right).\end{aligned} \tag{18}$$

The link transition rates $\beta^i(l \to j)$ for the PA equations (18) are obtained by inserting the PA ansatz into the AME link transition rates of (5), yielding

$$\beta^i(l \to j) = \frac{\langle x_k^l(t) \sum_{|\mathbf{m}|=k} m_i \mathrm{Mult}_{k,l}(\mathbf{m}) F_{\mathbf{m}}(l \to j) \rangle_k}{\langle x_k^l(t) k q_k^{l \to i}(t) \rangle_k}. \tag{19}$$

Thus, we have completely described the PA framework, which is comprised of (15) and (18) for $0 \le i, j \le n-1$ and for $k_{\min} \le k \le k_{max}$. This is a closed set of $(n^2+n)(k_{\max}-k_{\min}+1)$ equations that describes the evolution of the system from initial conditions $x_k^i(0)$ and $q_k^{i \to j}(0)$. Importantly, the size of the system scales linearly with the range $k_{\max}-k_{\min}$ of possible degrees, which is relatively modest compared to the size of the AME system of (10). This is especially relevant when studying networks with heterogeneous degree distributions, i.e., with large values of $k_{\max}-k_{\min}$.

3.3. Mean-Field Framework. In the mean-field (MF) approximation scheme it is assumed that the states of each node in the network are independent. Dynamical correlations that may exist between a node and its nearest neighbors are, as a result, neglected. To arrive at the MF equations from the PA framework, we note that the link probabilities $q_k^{i \to j}(t)$ are independent of i under the MF assumption. Thus, for all values of i, $q_k^{i \to j}(t)$ is replaced by $\omega^j(t)$, the MF probability that the neighbor of a node is in state j at time t. The value of $\omega_j(t)$ is approximated directly from the $x_k^i(t)$ terms by a global average of node states over the entire network, given by

$$\omega^j(t) = \sum_{k=0}^{\infty} \frac{k p_k}{z} x_k^j(t), \tag{20}$$

where $z = \langle k \rangle$ is the average degree of the network. In (20), kp_k/z is the probability that a neighbor of a node has degree k in the configuration network model, while $x_k^j(t)$ is the probability that such a neighbor is in state i. Summing over all possible values of neighbor degrees k gives the desired probability $\omega^j(t)$. The MF ansatz of (20) can be inserted into the PA evolution equation for x_k^i to give the MF evolution equation for $x_k^i(t)$:

$$\frac{d}{dt}x_k^i = -\sum_{j \ne i} x_k^i \sum_{|\mathbf{m}|=k} \mathrm{Mult}_k(\mathbf{m}) F_{\mathbf{m}}(i \to j) + \sum_{j \ne i} x_k^j \sum_{|\mathbf{m}|=k} \mathrm{Mult}_k(\mathbf{m}) F_{\mathbf{m}}(j \to i), \tag{21}$$

where, similar to (12), $\mathrm{Mult}_k(\mathbf{m})$ is defined as

$$\mathrm{Mult}_k(\mathbf{m}) = \frac{k!}{m_0! \dots m_{n-1}!} (\omega^0)^{m_0} \dots (\omega^{n-1})^{m_{n-1}}. \tag{22}$$

Equation (21), for $0 \le i \le n-1$ and $k_{\min} \le k \le k_{\max}$, is a closed system of $n(k_{\max}-k_{\min}+1)$ equations that describe the evolution of the MF dynamics from initial conditions $x_k^i(0)$. Note that the MF equations can be represented eloquently in vector form; if we denote by $\mathbf{x}_k(t)$ the $n \times 1$ vector whose ith entry is $x_k^i(t)$, then the evolution equation for $\mathbf{x}_k(t)$ is given by

$$\frac{d}{dt}\mathbf{x}_k = -\sum_{|\mathbf{m}|=k} \left(\mathbf{R}_{\mathbf{m}} - \mathbf{F}_{\mathbf{m}}^{\mathrm{T}}\right) \mathrm{Mult}_k(\mathbf{m}) \mathbf{x}_k, \tag{23}$$

where $\mathbf{F}_{\mathbf{m}}^T$ is the transpose of the transition rate matrix and $\mathbf{R}_{\mathbf{m}}$ is the diagonal matrix with elements $(\mathbf{R}_{\mathbf{m}})_{ii} = \sum_{j=1}^{n} F_{\mathbf{m}}(i \to j)$.

To recap, we have derived the AME, PA, and MF approximation frameworks by making a series of progressively stronger assumptions. The AME assumes that the transition rate of the neighbor of a given node is independent of the states of all other neighbors of the node. Note also that by closing the AME system of equations we explicitly assume independence between a node and all other nodes in the network beyond its nearest neighbors (i.e., an absence of long range correlations). The PA brings the level of approximation a step further by assuming that the *state* of the neighbor of a node is independent of the states of all other neighbors of the node, while the MF makes the strongest possible assumption with the ansatz that the state of every node in the network is independent.

3.4. Numerical Solvers. In sections 3.1 through 3.3 we have presented the AME, PA, and MF theoretical frameworks and have seen that the number of equations in the approximation frameworks markedly decreases as simplifying assumptions are made. While the AME scales superlinearly in both the number of states n and the maximum degree $k_{\max}$, the PA scales linearly in the range $k_{\max} - k_{\min}$ of the degree distribution, while the MF approximation scales linearly in both n and $k_{\max} - k_{\min}$. The latter frameworks can be attractive for exploring dynamical processes, as their relatively small system size lends itself to analytical study. However, the simplifying assumptions employed to arrive at such frameworks may result in a significant loss of accuracy or even a complete failure to capture the dynamics, and so there are cases when the higher accuracy approximation schemes, although possibly not solvable analytically, can give valuable qualitative and quantitative (through numerical solution) insights into the dynamics. For the cases where analytical solutions are not attainable, we make freely available a MATLAB/Octave package to numerically solve the systems of equations [20], which has been optimized to deal with the large number of equations that can occur, particularly in the case of the AME.

4. Analysis. In this section, we illustrate the power of the approximation frameworks introduced in section 3 in understanding multistate dynamical processes. We first illustrate our approach with the study of coevolving epidemiological dynamics, where two epidemic processes interact with each other on a network. Our equations reveal the rich equilibrium behavior of these dynamics and the interplay between the connectivity of the network and the infectivity parameters of the diseases. Following this we present a dynamical process from the physical sciences which displays jamming or segregation at equilibrium, and we demonstrate the necessity for high accuracy approximations for capturing such complex behavior.

4.1. Cooperative Disease Dynamics. The study of cooperative diseases, where one disease can facilitate the spread of another disease, is an area that is gaining much scientific attention [12, 37, 32, 59], motivated by the dependencies between real diseases such as HIV and tuberculosis [14]. The model we study here is a relatively simple model of two cooperative SIS processes which we label disease 1 and disease 2. In their individual behaviors (i.e., in the absence of the other disease), the diseases are identical: Individuals infected with a single disease transmit that disease to each of their neighbors at a rate β, while infected individuals recover at rate 1. Interaction between the two diseases occurs via the mechanism whereby individuals already infected with one disease are more likely to become infected with the other disease. A node infected with one disease will contract the other disease at a rate $\lambda\beta$ from each

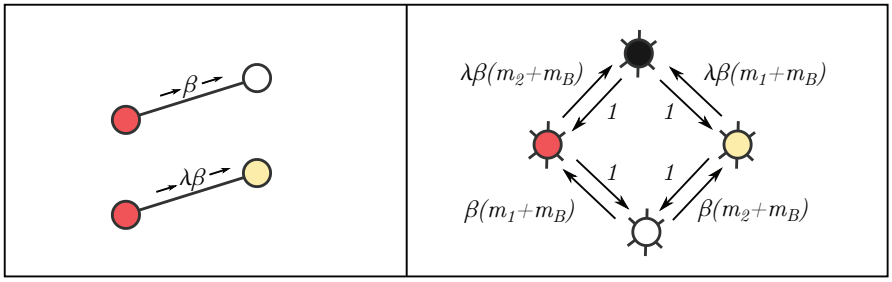

Fig. 3 *Schematic of the transition rates in the cooperative SIS model. In this model, individuals can be in one of four states: susceptible (white), infected with disease* 1 *(red), infected with disease* 2 *(yellow), or infected with both diseases (black). Left: A disease will be transmitted from a node with one disease to a susceptible node at a rate* β*, while it will be transmitted to a node that is infected with the other disease at an accentuated rate* $\lambda\beta$*. Right: The transition rates between the various states. Here,* m_1, m_2*, and* m_B *are the number of neighbors of the nodes with, respectively, disease* 1 *only, disease* 2 *only, and both diseases.*

of its neighbors that is infected with the other disease, where $\lambda \geq 1$ is an accentuation parameter quantifying the increased vulnerability of infected nodes relative to healthy nodes. The transitions in the model are illustrated in the schematic of Figure 3. This specific model has previously been studied analytically in the case of fully mixed populations [11, 12, 37], while also receiving limited analytical treatment in the case of clustered networks and their tree-like equivalents [32]. We also note that it is a special case of the very general ten-parameter model of coevolving SIS processes introduced by Sanz et al. [59]. The aim of our work here is to gain a full understanding of the dynamics of the model and the interplay between the disease parameters β and λ and the network connectivity characteristics, i.e., the degree distribution p_k.

In the absence of interaction (i.e., if $\lambda = 1$), each disease independently behaves as a traditional binary-state SIS process. For such processes, the critical value of β at which an endemic disease state persists in the population is given by degree-based MF theory [56] as

$$\beta_c = \frac{z}{\langle k^2 \rangle}, \tag{24}$$

where $\langle k^2 \rangle$ is the second moment of the degree distribution. The interesting question, then, is the effect that the interaction between the two diseases will have on the epidemic threshold β_c of each of the diseases. We examine this in detail through our degree-based frameworks with the aim of qualitatively exploring the state space (λ, β) in terms of the equilibrium behavior of the interacting diseases.

The coevolving disease model we have described above can be represented as a four-state model where each node is either susceptible (S), infected only with disease 1 (I_1), infected only with disease 2 (I_2), or infected with both diseases (B). The transitions of a node between states are encoded in the rate functions $F_{\mathbf{m}}(i \to j)$, where $\mathbf{m} = \{m_S, m_1, m_2, m_B\}$ is the number of neighbors a node has in the various states. These transitions are illustrated in Figure 3. Nodes infected with a disease recover from that disease at a rate 1, so $F_{\mathbf{m}}(I_1 \to S) = F_{\mathbf{m}}(I_2 \to S) = F_{\mathbf{m}}(B \to I_1) = F_{\mathbf{m}}(B \to I_2) = 1$. On the other hand, susceptible nodes will contract disease 1 from each of their m_1+m_B neighbors that are infected with disease 1 at a rate β, and disease 2 from each of their m_2+m_B neighbors that are infected with disease 2 at the same rate

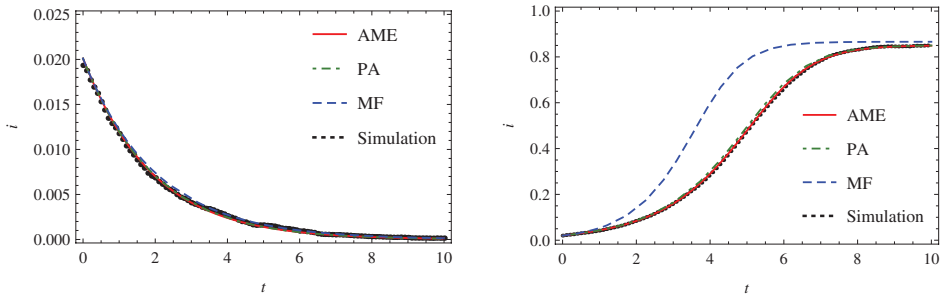

Fig. 4 *The expected fraction of infected nodes $i(t)$ in a degree-regular network ($z = 8$) with $\lambda = 2$ and $\beta = 0.5\beta_c$ (left) and $\beta = 2\beta_c$ (right), where $\beta_c = 1/8$ here is the prediction of the critical point for regular SIS dynamics as given by* (24)*. Each plot shows $i(t)$ as given by the AME, PA, and MF frameworks, as well as $i(t)$ attained through numerical simulations of the dynamics on a network of 10^4 nodes using a Gillespie algorithm* [25].

β; this gives $F_{\mathbf{m}}(S \to I_1) = (m_1 + m_B)\beta$ and $F_{\mathbf{m}}(S \to I_2) = (m_2 + m_B)\beta$. Nodes that are already infected with one disease contract the other disease at an accentuated rate $\lambda\beta$, thus $F_{\mathbf{m}}(I_1 \to B) = (m_1 + m_B)\lambda\beta$ and $F_{\mathbf{m}}(I_2 \to B) = (m_2 + m_B)\lambda\beta$. No further transitions are possible and so the transition rate matrix $\mathbf{F_m}$ for this cooperative SIS model is given by

$$\mathbf{F_m} = \begin{array}{c} \\ S \\ I_1 \\ I_2 \\ B \end{array} \begin{array}{c} \begin{array}{cccc} S & I_1 & I_2 & B \end{array} \\ \begin{pmatrix} 0 & (m_1+m_B)\beta & (m_2+m_B)\beta & 0 \\ 1 & 0 & 0 & (m_2+m_B)\lambda\beta \\ 1 & 0 & 0 & (m_1+m_B)\lambda\beta \\ 0 & 1 & 1 & 0 \end{pmatrix} \end{array}. \tag{25}$$

To begin, we study the evolution of the two diseases on a degree-regular random network, i.e., one in which every node has the same degree z so the degree distribution is $p_k = \delta_{k,z}$, and subsequently we examine the dynamics on networks with heterogeneous degree distributions. We analyze the expected fraction of infected individuals $i(t)$ in the population for different values of β and λ, where $i(t)$ includes all nodes with disease 1, disease 2, and both diseases. Figure 4 shows the time evolution of $i(t)$ for two values of β, one below and one above the single-disease epidemic threshold of (24), with the accentuation parameter taking the value $\lambda = 2$. We plot $i(t)$ from the AME, PA, and MF systems of equations as well as $i(t)$ constructed from numerical simulations, which throughout this work will be performed using the Gillespie algorithm [25, 22]. From Figure 4, it is clear that the AME and PA frameworks have an excellent level of accuracy, matching the numerical simulations to a high degree of accuracy above and below the critical point. Moreover, the MF framework, though deviating from the simulations in the transient regime for β above the critical point, is still quite accurate in the equilibrium regime ($t \to \infty$). Indeed, previous numerical studies have shown that MF frameworks can give highly accurate results for the equilibrium behavior of SIS dynamics [49]. We thus employ the MF framework for our analysis because of (a) its level of accuracy, and (b) its relative tractability over the PA and AME frameworks.

To begin our analysis using the MF framework of (21) on degree-regular networks we denote as x_z^S, x_z^1, x_z^2, and x_z^B the fraction of nodes in the network in each of the four states. Note we use the z subscript instead of k as every node in a degree-regular network has the same degree $k = z$. The evolution equations for x_z^S, x_z^1, x_z^2 and x_z^B are attained by inserting the rate functions $F_{\mathbf{m}}(i \to j)$ into (21). In (21), the rate functions are part of the expression

$$\sum_{|\mathbf{m}|=z} F_{\mathbf{m}}(i \to j)\mathrm{Mult}_z(\mathbf{m}, \omega), \tag{26}$$

where ω in the case of a degree-regular network is simply $\omega = \{x_z^S, x_z^1, x_z^2, x_z^B\}$. For the cases when $F_{\mathbf{m}}(i \to j) = 1$, as for the recovery transitions $I_1 \to S$, $I_2 \to S$, $B \to I_1$, and $B \to I_2$, (26) becomes

$$\sum_{|\mathbf{m}|=z} 1 \times \mathrm{Mult}_k(\mathbf{m}, \omega) = 1, \tag{27}$$

because the sum of multinomial probabilities over all possible events is equal to 1. For the infection transitions, we first consider the transition $S \to I_1$, which occurs at rate $F_{\mathbf{m}}(S \to I_1) = (m_1 + m_B)\beta$. In this case, (26) yields

$$\beta \sum_{|\mathbf{m}|=z} m_1 \mathrm{Mult}_z(\mathbf{m}, \omega) + \beta \sum_{|\mathbf{m}|=z} m_B \mathrm{Mult}_z(\mathbf{m}, \omega) = \beta z x_z^1 + \beta z x_z^B, \tag{28}$$

where we have used the first moment property of the multinomial distribution. Similar expressions are found for the transitions $S \to I_2$, $I_1 \to B$, $I_2 \to B$. Finally, inserting each of the appropriate transition rates into (21) gives the following system of MF evolution equations:

$$\frac{dx_z^S}{dt} = -\beta z(x_z^1 + x_z^B)x_z^S - \beta z(x_z^2 + x_z^B)x_z^S + x_z^1 + x_z^2, \tag{29}$$

$$\frac{dx_z^1}{dt} = -x_z^1 - \lambda\beta z(x_z^2 + x_z^B)x_z^1 + \beta z(x_z^1 + x_z^B)x_z^S + x_z^B, \tag{30}$$

$$\frac{dx_z^2}{dt} = -x_z^2 - \lambda\beta z(x_z^1 + x_z^B)x_z^2 + \beta z(x_z^2 + x_z^B)x_z^S + x_z^B, \tag{31}$$

$$\frac{dx_z^B}{dt} = -2x_z^B + \lambda\beta z(x_z^2 + x_z^B)x_z^1 + \lambda\beta z(x_z^1 + x_z^B)x_z^2. \tag{32}$$

Equations (29)–(32) form a closed system that describes the time evolution from initial conditions $x_z^S(0), x_z^1(0), x_z^2(0), x_z^B(0)$.

Of particular interest in epidemic dynamics is whether or not the disease eventually dies out, i.e., whether the population eventually become disease-free or whether it remains in an equilibrium endemic state. The equilibrium behavior of the dynamics can be analyzed by setting the time derivatives of (29)–(32) to zero and solving the resulting equations for $\bar{x}_z^S, \bar{x}_z^1, \bar{x}_z^2$, and $\bar{x}_z^B$, where the bar denotes steady-state values. The equilibrium states are summarized in the phase diagram of Figure 5, which shows the regions of (λ, β) space where qualitatively different equilibrium behavior occurs. We now describe these equilibrium states and the manner in which they are calculated.

The equilibrium behavior of the dynamics is analyzed in terms of the total fraction of infected nodes $\bar{i}$ in the network, where $\bar{i} = \bar{x}_z^1 + \bar{x}_z^2 + \bar{x}_z^B = 1 - \bar{x}_z^S$. If $\bar{i} = 0$,

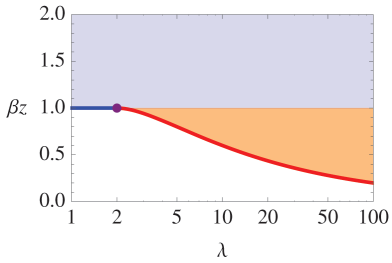

Fig. 5 *The phase diagram of the cooperative SIS model on a degree-regular network where each node has degree z. In all areas of the parameter space, the disease-free state exists. In the blue area above the line $\beta = 1/z$, the endemic state also exists and is the only stable equilibrium. In the orange region between the line $\beta = 1/z$ and the critical curve of* (36) *(thick red curve), both the endemic and disease-free states are stable, with the equilibrium state in this region depending on the initial conditions.*

both diseases eventually die out; otherwise, one or both diseases become endemic. The disease-free state is an equilibrium state that exists for all values of β and λ. However, depending on the values of β and λ, this equilibrium state may be either stable or unstable. In the case of an unstable disease-free state, any perturbation (i.e., any nonzero value of the initial infected fractions) will eventually lead to an endemic equilibrium state. The stability of the disease-free state is examined through the eigenvalues of the Jacobian matrix associated with the system of equations (29)–(32), evaluated at $x_z^S = 1$ and $x_z^1 = x_z^2 = x_z^B = 0$. The largest nonzero eigenvalue,[2] $e_{\max}$, is given by

$$e_{\max} = z\beta - 1, \tag{33}$$

and so the disease-free state is stable only if $\beta < 1/z$ which, we note, is independent of the accentuation parameter λ. Thus, for $\beta < 1/z$, the system will converge to the disease-free state when the initial conditions are sufficiently close to this state.

However, other stable endemic states can exist alongside the stable disease-free state in this area of the parameter space $\beta < 1/z$, and so an endemic state may be reached depending on the value of the initial conditions. To find the other equilibrium states, we solve the steady-state equations of (29)–(32). These equations yield $\bar{x}_z^B = (1 - \bar{x}_z^S)(1 - z\beta\bar{x}_z^S)/(1 + z\beta\bar{x}_z^S)$, $\bar{x}_z^1 = (1 - z\beta\bar{x}_z^S)/z\beta\lambda$ and $\bar{x}_z^2 = \bar{x}_z^1$, and along with the condition that $\bar{x}_z^S + \bar{x}_z^1 + \bar{x}_z^2 + \bar{x}_z^B = 1$, this results in two possible values for $\bar{i}$, given by

$$\bar{i}_+ = \frac{\lambda - 2}{2(\lambda - 1)} + \frac{\sqrt{(z\lambda\beta)^2 - 4(\lambda - 1)}}{2z\beta(\lambda - 1)}, \tag{34}$$

$$\bar{i}_- = \frac{\lambda - 2}{2(\lambda - 1)} - \frac{\sqrt{(z\lambda\beta)^2 - 4(\lambda - 1)}}{2z\beta(\lambda - 1)}. \tag{35}$$

Physically relevant values of $\bar{i}$ must be real and lie between 0 and 1; such solutions for $\bar{i}_+$ and $\bar{i}_-$ exist only if $(z\lambda\beta)^2 - 4(\lambda - 1) \geq 0$ and $\lambda \geq 2$. The epidemic threshold is

[2] Note that the zero eigenvalue always exists; however, this is an artificial eigenvalue arising from the fact that the system given by (29)–(32) along with the equation $\bar{x}_z^S + \bar{x}_z^1 + \bar{x}_z^2 + \bar{x}_z^B = 1$ is overspecified.

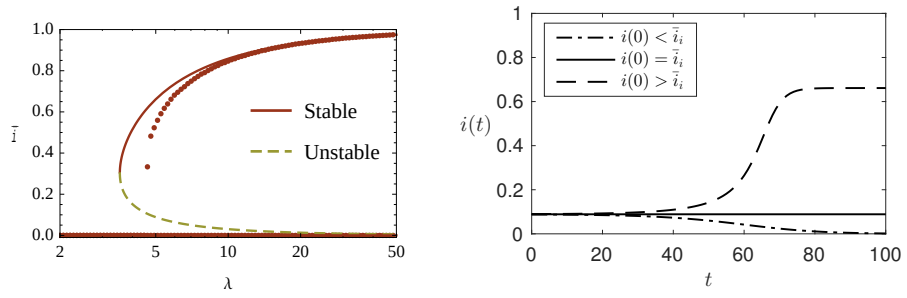

Fig. 6 *Behavior of the cooperative SIS model when the disease-free state is stable, i.e., $\beta < 1/z$. Here, the network is a degree-regular network where each node has degree $z = 8$, while β is fixed to the value $\beta = 0.9/z$. Left: The MF theory (curves) predicts the existence of a discontinuous transition when the accentuation parameter λ is increased above the critical point $\lambda_c(\beta)$, where $\lambda_c(\beta)$ is calculated by inverting* (36)*. Above this critical point there are three possible steady states: the disease-free stable state $\bar{i} = 0$, the unstable endemic state $\bar{i} = \bar{i}_-$, and the stable endemic state $\bar{i} = \bar{i}_+$. The qualitative accuracy of the MF predictions is confirmed here by numerical simulations (markers). Right: Evolution of the MF dynamics in the bistable regime $\lambda > \lambda_c(\beta)$ from initial conditions less than (dot-dashed curve), equal to (solid curve), and greater than (dashed curve) the unstable endemic state $\bar{i} = \bar{i}_-$, illustrating the reliance of the dynamics on initial conditions.*

therefore the smallest value of β for which these constraints are satisfied, and so the epidemic threshold β_c as a function of the accentuation parameter λ is given by

$$\beta_c(\lambda) = \frac{2\sqrt{\lambda - 1}}{z\lambda}, \qquad \lambda \geq 2. \tag{36}$$

This $\beta_c(\lambda)$ epidemic threshold curve is illustrated by the thick red curve in the phase diagram of Figure 5. Note that the value of $\beta_c(\lambda)$ is always less than $1/z$, which is the epidemic threshold in the absence of interaction from (24). It follows that interaction between the diseases lowers the value of the epidemic threshold, allowing endemic states to exist even when the infection transmission rates β are relatively small. Strikingly, the transition across this threshold is discontinuous, in contrast to the continuous transition that occurs in traditional SIS dynamics. At the point $\beta_c(\lambda)$ the fraction of infected nodes $\bar{i}$ can jump from zero to a finite value $(\lambda - 2)/2(\lambda - 1)$. This is illustrated in the left panel of Figure 6, which also shows how small changes in the value of λ—when close to the critical value $\lambda_c(\beta) = 2(1 + \sqrt{1 - (z\beta)^2})/(z\beta)^2$ obtained from inverting (36)—can trigger large changes in the macroscopic behavior of the system.

Previously, we saw that the disease-free state was unstable when $\beta > 1/z$. In this region of the parameter space, only one of the two solutions given by (35), the $\bar{i}_+$ solution, is physically meaningful. This is the stable solution, and so for any initial condition satisfying $x_z^S(0) < 1$ the equilibrium fraction of infected nodes will be given by $\bar{i}_+$. In the region of parameter space given by $\beta_c(\lambda) < \beta < 1/z$, both the $\bar{i}_+$ and $\bar{i}_-$ solutions exist and there are two stable states, the disease-free state and the endemic state $\bar{i}_+$, along with the unstable state $\bar{i}_-$. Here, the initial conditions of the system affect the steady state, as initial values $i(0) < \bar{i}_-$ will tend to the disease-free state and values $i(0) > \bar{i}_-$ will tend to the endemic state. The right panel of Figure 6 illustrates this behavior, showing how the dynamics evolve to the three different steady states from three different initial conditions, $i(0) > \bar{i}_-$, $i(0) = \bar{i}_-$, and $i(0) < \bar{i}_-$. It is

also noteworthy that the unstable steady state $\bar{i}_-$ tends monotonically to zero as a function of λ as $\mathcal{O}(\lambda^{-1})$ for large λ (as seen from (35)), indicating that for large values of λ the disease-free state will only be reached if the initial seed fraction of infected nodes is negligibly small.

The multistate MF framework of (21) has given us key insights into the behavior of cooperative SIS dynamics on degree-regular networks. The most notable property of the dynamics revealed by our analysis is the existence of a bistable equilibrium regime in which both a disease-free stable state and an endemic stable state exist, and the discontinuous transition that can occur upon entering this area of the parameter space. The simplicity of the model and of the MF framework has been beneficial for several reasons. First, certain analyses of more complicated, multiparameter models of cooperative SIS processes—of which this model is a special case—have not revealed the existence of discontinuous-transition behavior, as the large dimensionality of the system can be restrictive in finding this type of behavior [59]. Second, cases where discontinuous behavior has been identified have been largely restricted to study by numerical simulations [32], and the understanding that this gives regarding the behavior of the system in the bistable regime is limited. The MF analysis not only reveals the discontinuous transitions associated with cooperative SIS dynamics—and the approximate locations in parameter space at which these transitions occur—but it also gives analytical expressions for both the stable and the unstable equilibrium states in the bistable equilibrium regime, therefore increasing understanding of the behavior in the bistable regime.

The knowledge of the unstable state is of particular importance, as it dictates the final equilibrium state that the system will reach and gives a measure of the size of the perturbation required to shift the system from the disease-free state to the endemic state. This perturbation must be quite large for values of λ close to the critical point, and so the system should stay robustly in the disease-free state for such relatively small values of λ. However, the size of the required perturbation decreases to zero as λ increases, and so for sufficiently large values of λ only small perturbations from the disease-free state are required to move the system into the state of a large endemic outbreak. Our analysis has therefore given very detailed insights into the potential for catastrophic-type behavior in cooperative SIS dynamics, and such behavior has implications for the prediction and control of real diseases that interact in a cooperative manner [23, 63].

To complete our study of the cooperative SIS model, we examine the effect of heterogeneity in the degree distribution on the dynamics of the system. In Appendix A, we show that degree heterogeneity *promotes* the existence of an endemic state. There, we derive the critical point

$$\beta_c = \frac{z}{\langle k^2 \rangle}, \tag{37}$$

where for values $\beta > \beta_c$ the endemic state will always exist. This condition of (37) implies that $\beta_c \to 0$ for networks with degree distributions such that $\langle k^2 \rangle \to \infty$ (such as power-law distributions $p_k \propto k^{-\gamma}$ for $2 < \gamma < 3$). In such cases, the endemic state will exist for any value $\beta > 0$ and thus these networks are highly susceptible to endemic outbreaks. Interestingly, the threshold condition of (37) does not depend on λ, and so in networks with $\langle k^2 \rangle \to \infty$ even small values $\lambda \ll 1$ (in which case infection with one disease implies relative immunity toward the other) will not constrain an outbreak.

4.2. Kinetically Constrained Dynamics and the Necessity of High Accuracy Frameworks. In section 4.1 the multistate MF equations accurately captured the dynamics of the cooperative disease model of (25), providing a basis for insightful analysis into the behavior of the model. However, MF approximation frameworks do not always provide a sufficient level of accuracy, as the assumption of dynamical independence between each node in the network may be too strong. Higher accuracy frameworks such as the PA and the AME are required in such cases to provide tools for analysis, and we now illustrate this point with the study of a complex spin glass model from the physical sciences domain.

The Fredrickson–Andersen (FA) model is a spin model of glass-forming liquids [24], liquids that when supercooled from high temperatures can form crystalline structures [6]. In the FA model, a lattice or network represents the physical substrate, with nodes in the network having a spin which is either positive (+1) or negative (−1) representing dense and sparse areas of the substrate, respectively. A node's state can change dynamically over time but does so according to a kinetic constraint: state changes can only occur if the number of neighbors of a node with negative spin is greater than or equal to f, where f is the so-called facilitation parameter of the system. This kinetic constraint mechanism mimics jamming, where nodes can only be active (mobile) if they have space to do so because of a sufficiently large number of spin −1 ("sparse") neighbors. Once this constraint is met, nodes with spin −1 will change to spin +1 at a rate 1, while nodes with spin +1 will change to spin −1 at a rate $e^{-1/T}$; the latter rate is less than one and so the system favors the existence of spin +1 nodes. Here T is the temperature of the system. Combining the kinetic constraint with the spin flip rates gives the state transition rates of the system:

$$F_{\mathbf{m}}(-1 \to +1) = H(m_{-1} - f), \tag{38}$$

$$F_{\mathbf{m}}(+1 \to -1) = H(m_{-1} - f) \times e^{-1/T}, \tag{39}$$

where $H(x)$ is the Heaviside step function that takes the value $H(x) = 1$ for nonnegative values of x, and zero otherwise.

The FA model is one of a class of facilitated spin models, so called because mobile nodes (i.e., nodes that are not jammed) can facilitate the mobilization of other nodes that are jammed as a result of the kinetic constraint. In this fashion, facilitation can recursively cause the mobilization of jammed nodes and the relaxation of the system, in which case the resulting equilibrium state is the liquid state. On the other hand, the system may not fully relax, with jammed nodes occupying much of the substrate. This is the glass state, where the system is in dynamical arrest consisting of both mobile and frozen nodes. The final equilibrium state depends heavily on the temperature T, with a critical temperature T_c separating the liquid phase ($T > T_c$) and the arrested glassy phase ($T_c < T$) (see Figure 7). The essential quantity or order parameter that defines such states is the fraction Φ of frozen nodes in the system at equilibrium, with $\Phi = 0$ in the liquid state and $\Phi > 0$ in the glassy state.

In [21] we showed that despite the fact that the FA dynamics have nodes with only two possible spins +1 or −1, binary-state theoretical frameworks, including the high-accuracy two-state AME of [26, 27], incorrectly predict the equilibrium value of Φ to be zero for all values of the temperature, thus failing to capture the existence of the glassy phase at low temperatures. We therefore extended the state space of the dynamics to four states by including an auxiliary state c or u for each node that defines whether the node's spin state has changed since $t = 0$ (c) or is as yet unchanged (u).

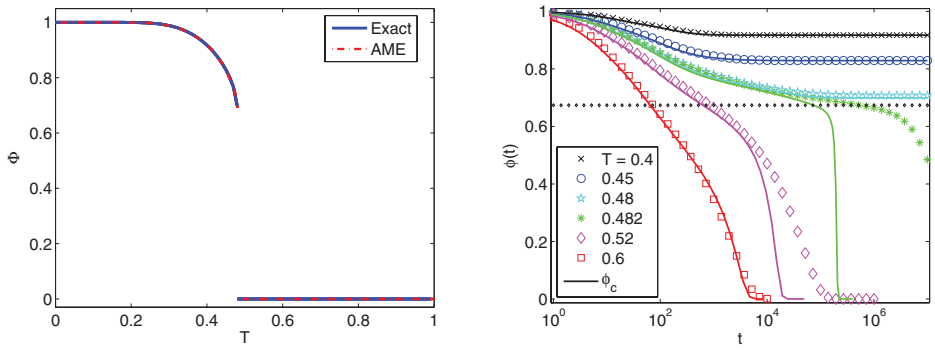

Fig. 7 *Behavior of the FA model on degree-regular networks ($z = 4$) with facilitation parameter $f = 2$ for various values of the temperature parameter T. Left: A discontinuous transition of the equilibrium order parameter occurs as the temperature T is reduced below the critical temperature T_c. The exact solution here is the equilibrium branching process approach on tree-like networks presented by Sellito et al.* [61]. *Right: The four-state AME (solid lines) captures the transient behavior of the FA model (symbols show numerical simulation results), recreating both the glassy and the liquid states. The transient variable $\phi(t)$ here is the fraction of frozen spins in the network at time t, with $\lim_{t\to\infty}\phi(t) = \Phi$.*

The corresponding rate matrix function for the four-state dynamics is

(40)
$$\mathbf{F_m} = \begin{array}{c} \\ (-1,u) \\ (+1,u) \\ (-1,c) \\ (+1,c) \end{array} \begin{array}{c} \begin{array}{cccc} (-1,u), & (+1,u) & (-1,c) & (+1,c) \end{array} \\ \begin{pmatrix} 0 & 0 & 0 & 1 \\ 0 & 0 & e^{-1/T} & 0 \\ 0 & 0 & 0 & 1 \\ 0 & 0 & e^{-1/T} & 0 \end{pmatrix} \end{array} * H(m_{(-1,u)} + m_{(-1,c)} - f).$$

By solving the system of equations given by (10), we found that the four-state AME can capture the essential dynamics of the system to a high level of accuracy. The four-state AME not only qualitatively predicts the existence of two equilibrium phases corresponding to liquid and glass, but also provides accurate predictions of the critical temperature T_c that separates the two phases and the values of the order parameter Φ in the glassy phase (see Figure 7, left panel). Furthermore, the four-state AME accurately reproduces the transient dynamics of the system (see Figure 7, right panel), a challenging task due to the long range correlations between distant nodes at temperatures close to the critical point T_c. The four-state AME captures the spatial heterogeneity of the dynamics in the glass phase, including the clustering of mobile and blocked nodes, which results in "patchy" equilibrium configurations.

On the contrary, the rich behavior of the FA model cannot be captured by the four-state PA and MF frameworks. Like their binary-state counterparts, these frameworks fail to reproduce the frozen glassy state, predicting that the fraction of frozen nodes Φ at equilibrium is zero for all values of the temperature T. We illustrate this by examining the system at a temperature $T < T_c$ as shown in Figure 8. Here, the fraction of frozen nodes in the system as predicted by the AME converges to the equilibrium value $\Phi \approx 0.91$, a value matched closely by numerical simulation of the dynamics. This value is positive, indicating that the system is in the glassy phase.

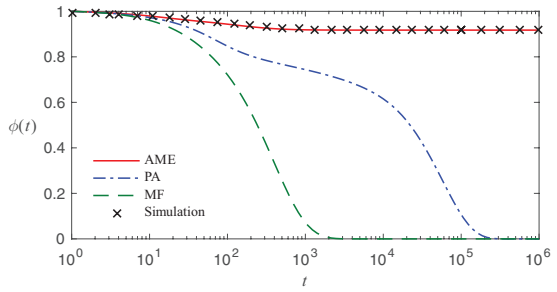

Fig. 8 *Comparison of the AME, PA, and MF frameworks for transient FA dynamics. As in Figure 7, the network is degree-regular ($z = 4$) with facilitation parameter $f = 2$. The temperature here is chosen to be below the critical point ($T = 0.4$). The AME matches excellently to the numerical simulation results, while the MF and PA frameworks fail to capture the model behavior. These qualitative observations hold for all values $T < T_c$.*

However, the fraction of frozen nodes as predicted by both the PA and MF frameworks converges to $\Phi = 0$, thus predicting that the system is in the liquid phase. Examination of the four-state MF and PA equations indicates that $\Phi > 0$ is not a possible equilibrium for any value of the temperature T, and thus they are insufficient for the study of these rich dynamics.

So why does the four-state AME capture the dynamics of the FA model while the four-state PA and MF frameworks do not? The answer lies in the nonlinear relationship between the states of nodes and the states of their neighbors. The AME variables $x^i_{\mathbf{m}}$ capture the relationship between a node and all of its neighbors, while the PA and MF frameworks approximate this relationship by link relationships and the multinomial distribution as given by (13), (12), and (22). Analysis of the AME equations for the FA model reveals nonlinear relationships; specifically, the variables $x^{(-1,u)}_{\mathbf{m}}$ and $x^{(+1,u)}_{\mathbf{m}}$ satisfy

$$x^{(-1,u)}_{\mathbf{m}}, x^{(+1,u)}_{\mathbf{m}} \text{ are } \begin{cases} = 0 & \text{if } m_{(-1,u)} + m_{(-1,c)} \geq f, \\ > 0 & \text{if } m_{(-1,u)} + m_{(-1,c)} < f. \end{cases} \tag{41}$$

This nonlinear relationship cannot be captured by the multinomial distribution approximation, whose values vary smoothly as a function of $m_{(-1,u)} + m_{(-1,c)}$. Indeed, the nonlinearity is essential for the freezing mechanism. The variables $x^{(-1,u)}_{\mathbf{m}}$ and $x^{(+1,u)}_{\mathbf{m}}$ cannot be nonzero for $m_{(-1,u)} + m_{(-1,c)} \geq f$ (as otherwise they are mobile and will change state from u to c), while they must be nonzero for $m_{(-1,u)} + m_{(-1,c)} < f$ to allow for the existence of a nonzero fraction of frozen nodes in the glassy regime. The four-state PA and MF frameworks do not account for this nonlinearity, and as a result their evolution equations for $x^{(-1,u)}_k$ and $x^{(+1,u)}_k$ do not reach a steady state until $x^{(-1,u)}_k = x^{(+1,u)}_k$, thus eliminating the possibility of a glassy equilibrium state.

Interestingly, our analysis here can be related to earlier results presented by Gleeson in [27] when examining binary-state AME, PA, and MF frameworks. There, the equilibrium states of the PA and AME frameworks were equivalent for a spin model known as the Ising model, a model that can recover the FA model in the absence of kinetic constraint (i.e., $f \to \infty$). However, the AME was the only framework capable of capturing the dynamics of threshold models which, as described in section 2, have

similar constraints to the FA model on state changing. The introduction of the kinetic constraint in the FA model has a large effect on the complexity of the dynamics and thus on the ability of various approximation frameworks to adequately capture its dynamics. Our observations here have important implications for the study of models with kinetic constraints. Threshold models are widely employed models of complex contagion in the social sciences [30, 10, 52, 36], and the AME framework that we have introduced here lends itself to the analysis of the traditional binary-state threshold models [71] as well as more complex multistate threshold models that are the focus of much current attention [51, 41].

5. Conclusions. In this paper we have derived degree-based approximation frameworks for the analysis of a wide class of multistate Markovian dynamical processes that can be defined in terms of rate matrix functions $\mathbf{F_m}$. These frameworks provide a comprehensive set of tools for the analysis of multistate dynamical processes on networks and can be used to study specific dynamics through an appropriate expression of a rate matrix function.

The multistate frameworks we have introduced are of varying levels of accuracy, and this provides flexibility in the choice of framework that should be employed when studying a dynamical process. High accuracy frameworks can be used to study complex processes whose dynamics cannot be captured by lower accuracy methods, a feature that we illustrated through our analysis of the Fredrickson–Andersen model of glassy dynamics in section 4.2. On the other hand, lower accuracy frameworks such as mean-field, when capable of capturing the essential aspects of the dynamics, can be sufficiently tractable to allow for analytical insight. The power of such analytically tractable frameworks has been illustrated in our study of the cooperative disease model in section 4.1, as the mean-field framework provides understanding of the combined effect of the dynamical parameters and the network connectivity on the equilibrium behavior of the dynamics.

We believe that our multistate frameworks provide a useful contribution to the field of dynamical processes on networks, and thus to the understanding of real dynamics in a wide range of applications. Furthermore, we have made optimized code available to produce numerical solutions to the equations of the approximation frameworks [20], giving our work an extra level of accessibility for the community at large.

Appendix A. Calculation of the Cooperative SIS Epidemic Threshold on Networks with Heterogeneous Degree Distributions. In this appendix, we examine the behavior of the cooperative SIS model as defined in section 4.1 on networks with heterogeneous degree distributions p_k. The MF equations for this system are obtained by inserting the rate function of (25) into (21); this gives the set of equations

$$\frac{dx_k^S}{dt} = -\beta k(w^{I_1} + w^B)x_k^S - \beta k(w^{I_2} + w^B)x_k^S + x_k^{I_1} + x_k^{I_2}, \tag{42}$$

$$\frac{dx_k^{I_1}}{dt} = -x_k^{I_1} - \lambda\beta k(w^{I_2} + w^B)x_k^{I_1} + \beta k(w^{I_1} + w^B)x_k^S + x_k^B, \tag{43}$$

$$\frac{dx_k^{I_2}}{dt} = -x_k^{I_2} - \lambda\beta k(w^{I_1} + w^B)x_k^{I_2} + \beta k(w^{I_2} + w^B)x_k^S + x_k^B, \tag{44}$$

$$\frac{dx_k^B}{dt} = -2x_k^B + \lambda\beta k(w^{I_2} + w^B)x_k^{I_1} + \lambda\beta k(w^{I_1} + w^B)x_k^{I_2}, \tag{45}$$

which holds for all values $k_{\min} \leq k \leq k_{\max}$. To analyze the system, we employ the

change of variables

$$x_k^S \leftarrow x_k^S, \tag{46}$$

$$y_k \leftarrow x_k^{I_2} + x_k^{I_1}, \tag{47}$$

$$\Delta_k \leftarrow x_k^{I_2} - x_k^{I_1}, \tag{48}$$

$$x_k^B \leftarrow x_k^B, \tag{49}$$

in which case we arrive at the set of equations

$$\frac{dx_k^S}{dt} = -\beta k(w^y + 2w^B)x_k^S + y_k, \tag{50}$$

$$\frac{dy_k}{dt} = -y_k - \lambda\beta k\left(\frac{w^y y_k - w^\Delta \Delta_k}{2} + w^B y_k\right) + \beta k(w^y + 2w^B)x_k^S + 2x_k^B, \tag{51}$$

$$\frac{d\Delta_k}{dt} = -\Delta_k - \lambda\beta k\left(\frac{w^y \Delta_k - w^\Delta y_k}{2} + w^B \Delta_k\right) + \beta k w^\Delta x_k^S, \tag{52}$$

$$\frac{dx_k^B}{dt} = -2x_k^B + \lambda\beta k\left(\frac{w^y y_k - w^\Delta \Delta_k}{2} + w^B y_k\right). \tag{53}$$

Using the property $x_k^B = 1 - x_k^S - y_k$ (and thus $w^B = 1 - w^S - w^y$), and restricting the equations to the steady state, we have the following system of equations which allow for the analysis of the equilibrium behavior:

$$0 = -\beta k(2 - 2w^S - w^y)x_k^S + y_k, \tag{54}$$

$$\begin{aligned} 0 = {} & -y_k - \lambda\beta k\left((1 - w^S)y_k - \frac{w^y y_k + w^\Delta \Delta_k}{2}\right), \\ & + \beta k(2 - 2w^S - w^y)x_k^S + 2(1 - x_k^S - y_k), \end{aligned} \tag{55}$$

$$0 = -\Delta_k - \lambda\beta k\left((1 - w^S)\Delta_k - \frac{w^y \Delta_k + w^\Delta y_k}{2}\right) + \beta k w^\Delta x_k^S. \tag{56}$$

From (54) we obtain expressions for y_k and w^y in terms of the other variables as

$$y_k = 2\frac{\beta k(1 - w^S)}{1 + \beta U_S}x_k^S, \tag{57}$$

$$w^y = 2\frac{(1 - w^S)\beta U_S}{1 + \beta U_S}, \tag{58}$$

where $U_S = \sum_k (kp_k/z)x_k^S$, while (56) lets us isolate Δ_k as

$$\Delta_k = \frac{\beta k w^\Delta \left(1 + \lambda\beta k \frac{1 - w^S}{1 + \beta U_s}\right)}{1 + \lambda\beta k \frac{1 - w^S}{1 + \beta U_s}}x_k^S = \beta k w^\Delta x_k^S. \tag{59}$$

Finally, y_k, w^y, and Δ_k can be inserted into (55) to give

$$0 = \left(-\left(\lambda\beta k\frac{1 - w^S}{1 + \beta U_s} + 2\right)\left(\frac{\beta k(1 - w^S)}{1 + \beta U_s}\right) + \left(\left(\lambda\beta k\frac{w^\Delta}{4}\right)\beta k w^\Delta\right) - 1\right)x_k^S + 1, \tag{60}$$

and thus we have that

$$x_k^S = \frac{1}{1 + 2\frac{\beta k(1-w^S)}{1+\beta U_s} + \lambda(\beta k)^2 \left(\left(\frac{1-w^S}{1+\beta U_s} \right)^2 - \left(\frac{w^\Delta}{2} \right)^2 \right)} \tag{61}$$

and

$$w^S = \sum_k \frac{kp_k}{z} \frac{1}{1 + 2\frac{\beta k(1-w^S)}{1+\beta U_s} + \lambda(\beta k)^2 \left(\left(\frac{1-w^S}{1+\beta U_s} \right)^2 - \left(\frac{w^\Delta}{2} \right)^2 \right)}. \tag{62}$$

We can see that $w^S = 1$ (in which case $w^\Delta = 0$) is a solution to (62). This is the trivial solution that always exists, in which case every node in the network is healthy. We search for an endemic solution $0 \leq w^S < 1$ by subtracting 1 from both sides of (62) and dividing by $w^S - 1$, giving

$$1 = \sum_k \frac{kp_k}{z} \frac{2\frac{\beta k}{1+\beta U_s} + \lambda(\beta k)^2 \left(\frac{1-w^S}{(1+\beta U_s)^2} - \frac{1}{1-w^S} \left(\frac{w^\Delta}{2} \right)^2 \right)}{1 + 2\frac{\beta k(1-w^S)}{1+\beta U_s} + \lambda(\beta k)^2 \left(\left(\frac{1-w^S}{1+\beta U_s} \right)^2 - \left(\frac{w^\Delta}{2} \right)^2 \right)}. \tag{63}$$

Now, to see if there is a solution $0 \leq w^S < 1$ to (63), we examine the right hand side of (63) at the limits $w^S = 0$ and $w^S \to 1$; a solution is guaranteed to exist if one of these values is less than 1 and one of them greater than 1 (as (63) is a continuous function of w^S). The right hand side of (63) in the limit $w^S \to 1$ (and so $U_s \to \langle k^2 \rangle / z$ and $w^\Delta \to 0$) is

$$\lim_{w^S \to 1} rhs(w^S) = \sum_k \frac{kp_k}{z} \left(\frac{2\beta k}{1 + \beta \langle k^2 \rangle / z} + \frac{\lambda(\beta k)^2}{4} \lim_{w^S \to 1} \frac{\left(w^\Delta\right)^2}{1 - w^S} \right). \tag{64}$$

Now

$$\left(w^\Delta\right)^2 = \left(\sum_k \frac{kp_k}{z} (x_k^{I_2} - x_k^{I_1}) \right)^2 \leq \left(\sum_k \frac{kp_k}{z} \max(x_k^{I_2}, x_k^{I_1}) \right)^2 \tag{65}$$

and

$$1 - w^S = \sum_k \frac{kp_k}{z} (x_k^{I_1} + x_k^{I_2} + x_k^B) \geq \sum_k \frac{kp_k}{z} \max(x_k^{I_2}, x_k^{I_1}), \tag{66}$$

and so

$$\lim_{w^S \to 1} \frac{\left(w^\Delta\right)^2}{1 - w^S} \leq \lim_{w^S \to 1} \frac{\left(\sum_k \frac{kp_k}{z} \max(x_k^{I_2}, x_k^{I_1}) \right)^2}{\sum_k \frac{kp_k}{z} \max(x_k^{I_2}, x_k^{I_1})} \tag{67}$$

$$= \lim_{w^S \to 1} \sum_k \frac{kp_k}{z} \max(x_k^{I_2}, x_k^{I_1}) = 0, \tag{68}$$

as $x_k^{I_1}, x_k^{I_2} \to 0$ when $w^S \to 1$. Thus, from (64) we have that

$$\lim_{w^S \to 1} rhs(w^S) = \sum_k \frac{kp_k}{z} \frac{2\beta k}{1 + \beta \langle k^2 \rangle / z} \tag{69}$$

$$= \frac{2\beta \langle k^2 \rangle / z}{1 + \beta \langle k^2 \rangle / z}. \tag{70}$$

On the other hand, in the case that $w^S = 0$ (and so $U_s = 0$) we have

$$rhs(w^S = 0) = \sum_k \frac{kp_k}{z} \frac{2\beta k + \lambda(\beta k)^2 \left(1 - \left(\frac{w^\Delta}{2}\right)^2\right)}{1 + 2\beta k + \lambda(\beta k)^2 \left(1 - \left(\frac{w^\Delta}{2}\right)^2\right)} < 1. \tag{71}$$

Since $rhs(w^S = 0) < 1$, then a solution of (63) with $0 \leq w^S < 1$ is guaranteed to exist if $rhs(w^S \to 1) > 1$; from (70) this occurs when

$$\beta > \frac{z}{\langle k^2 \rangle}. \tag{72}$$

Thus, we have derived the threshold condition, and so when the infection parameter β satisfies (72) there will always exist an endemic state.

Acknowledgments. We acknowledge helpful discussions with Fakhteh Ghanbarnejad and Davide Cellai.

REFERENCES

[1] C. L. Althaus, *Estimating the reproduction number of Ebola virus (EBOV) during the* 2014 *outbreak in West Africa*, PLoS Currents, 6 (2014). (Cited on p. 94)

[2] R. M. Anderson, R. M. May, and B. Anderson, *Infectious Diseases of Humans: Dynamics and Control*, Vol. 28, Wiley Online Library, 1992. (Cited on p. 94)

[3] D. Balcan, B. Gonçalves, H. Hu, J. J. Ramasco, V. Colizza, and A. Vespignani, *Modeling the spatial spread of infectious diseases: The global epidemic and mobility computational model*, J. Comput. Sci., 1 (2010), pp. 132–145. (Cited on p. 93)

[4] A. Barrat, M. Barthelemy, and A. Vespignani, *Dynamical Processes on Complex Networks*, Cambridge University Press, 2008. (Cited on p. 92)

[5] F. M. Bass, *A new product growth for model consumer durables*, Management Sci., 15 (1969), pp. 215–227. (Cited on p. 92)

[6] G. Biroli and J.-P. Bouchaud, *The random first-order transition theory of glasses: A critical assessment*, in Structural Glasses and Supercooled Liquids: Theory, Experiment, and Applications, P. G. Wolynes and V. Lubchenko, eds., John Wiley & Sons, 2012, pp. 31–113. (Cited on p. 109)

[7] C. Castellano, S. Fortunato, and V. Loreto, *Statistical physics of social dynamics*, Rev. Modern Phys., 81 (2009), art. 591. (Cited on p. 95)

[8] X. Castelló, A. Baronchelli, and V. Loreto, *Consensus and ordering in language dynamics*, European Phys. J. B, 71 (2009), pp. 557–564. (Cited on p. 95)

[9] C. Castillo-Chavez and B. Song, *Models for the transmission dynamics of fanatic behaviors*, Bioterrorism, 28 (2003), pp. 155–172. (Cited on p. 95)

[10] D. Centola and M. Macy, *Complex contagions and the weakness of long ties*, Amer. J. Sociology, 113 (2007), pp. 702–734. (Cited on pp. 96, 112)

[11] L. Chen, F. Ghanbarnejad, and D. Brockmann, *Fundamental properties of cooperative contagion processes*, New J. Phys., 19 (2017), art. 103041. (Cited on p. 103)

[12] L. Chen, F. Ghanbarnejad, W. Cai, and P. Grassberger, *Outbreaks of coinfections: The critical role of cooperativity*, Europhys. Lett., 104 (2013), art. 50001. (Cited on pp. 95, 102, 103)

[13] P. Chen and S. Redner, *Consensus formation in multi-state majority and plurality models*, J. Phys. A, 38 (2005), pp. 7239–7252. (Cited on p. 96)

[14] E. L. Corbett, C. J. Watt, N. Walker, D. Maher, B. G. Williams, M. C. Raviglione, and C. Dye, *The growing burden of tuberculosis: Global trends and interactions with the HIV epidemic*, Arch. Internal Medicine, 163 (2003), pp. 1009–1021. (Cited on pp. 95, 102)

[15] L. Dall'Asta and C. Castellano, *Effective surface-tension in the noise-reduced voter model*, Europhys. Lett., 77 (2007), art. 60005. (Cited on p. 95)

[16] G. F. de Arruda, F. A. Rodrigues, P. M. Rodriiguez, E. Cozzo, and Y. Moreno, *Unifying Markov Chain Approach for Disease and Rumor Spreading in Complex Networks*, preprint, https://arxiv.org/abs/1609.00682, 2016. (Cited on pp. 93, 95)

[17] M. Draief, A. Ganesh, and L. Massoulié, *Thresholds for virus spread on networks*, in Proceedings of the 1st International Conference on Performance Evaluation Methodologies and Tools, ACM, 2006, art. 51. (Cited on p. 94)
[18] J. Dushoff, J. B. Plotkin, S. A. Levin, and D. J. Earn, *Dynamical resonance can account for seasonality of influenza epidemics*, Proc. Natl. Acad. Sci. USA, 101 (2004), pp. 16915–16916. (Cited on p. 94)
[19] W. Feller, *An Introduction to Probability Theory and its Applications*, Vol. 2, John Wiley & Sons, 2008. (Cited on p. 99)
[20] P. G. Fennell, *Multistate ODE Solver*, Version 1.0, 2016, https://github.com/peterfennell/multi-state-SOLVER. (Cited on pp. 102, 112)
[21] P. G. Fennell, J. P. Gleeson, and D. Cellai, *Analytical approach to the dynamics of facilitated spin models on random networks*, Phys. Rev. E, 90 (2014), art. 032824. (Cited on pp. 96, 109)
[22] P. G. Fennell, S. Melnik, and J. P. Gleeson, *Limitations of discrete-time approaches to continuous-time contagion dynamics*, Phys. Rev. E, 94 (2016), art. 052125. (Cited on pp. 95, 104)
[23] D. T. Fleming and J. N. Wasserheit, *From epidemiological synergy to public health policy and practice: The contribution of other sexually transmitted diseases to sexual transmission of HIV infection*, Sexually Transmitted Infections, 75 (1999), pp. 3–17. (Cited on p. 108)
[24] G. H. Fredrickson and H. C. Andersen, *Kinetic Ising model of the glass transition*, Phys. Rev. Lett., 53 (1984), p. 1244. (Cited on p. 109)
[25] D. T. Gillespie, *Exact stochastic simulation of coupled chemical reactions*, J. Phys. Chem., 81 (1977), pp. 2340–2361. (Cited on p. 104)
[26] J. P. Gleeson, *High-accuracy approximation of binary-state dynamics on networks*, Phys. Rev. Lett., 107 (2011), art. 068701. (Cited on pp. 96, 109)
[27] J. P. Gleeson, *Binary-state dynamics on complex networks: Pair approximation and beyond*, Phys. Rev. X, 3 (2013), art. 021004. (Cited on pp. 92, 93, 96, 109, 111)
[28] M. F. Gomes, A. Piontti, L. Rossi, D. Chao, I. Longini, M. E. Halloran, and A. Vespignani, *Assessing the international spreading risk associated with the* 2014 *West African Ebola outbreak*, PLOS Currents Outbreaks, 1 (2014). (Cited on pp. 93, 94)
[29] C. Granell, S. Gómez, and A. Arenas, *Dynamical interplay between awareness and epidemic spreading in multiplex networks*, Phys. Rev. Lett., 111 (2013), art. 128701. (Cited on p. 95)
[30] M. S. Granovetter, *The strength of weak ties*, Amer. J. Sociology, 78 (1973), pp. 1360–1380. (Cited on p. 112)
[31] H. Guo, M. Y. Li, and Z. Shuai, *Global dynamics of a general class of multistage models for infectious diseases*, SIAM J. Appl. Math., 72 (2012), pp. 261–279, https://doi.org/10.1137/110827028. (Cited on p. 94)
[32] L. Hébert-Dufresne and B. M. Althouse, *Complex dynamics of synergistic coinfections on realistically clustered networks*, Proc. Natl. Acad. Sci. USA, 112 (2015), pp. 10551–10556. (Cited on pp. 95, 102, 103, 108)
[33] H. Hethcote, M. Zhien, and L. Shengbing, *Effects of quarantine in six endemic models for infectious diseases*, Math. Biosci., 180 (2002), pp. 141–160. (Cited on p. 94)
[34] H. W. Hethcote, *The mathematics of infectious diseases*, SIAM Rev., 42 (2000), pp. 599–653, https://doi.org/10.1137/S0036144500371907. (Cited on pp. 93, 94)
[35] M. B. Hooten, J. Anderson, and L. A. Waller, *Assessing North American influenza dynamics with a statistical SIRS model*, Spatial Spatio-Temporal Epidemiology, 1 (2010), pp. 177–185. (Cited on p. 94)
[36] G. Iñiguez, Z. Ruan, K. Kaski, J. Kertész, and M. Karsai, *Service adoption spreading in online social networks*, in Complex Spreading Phenomena in Social Systems, Springer, Cham, 2018, pp. 151–175. (Cited on p. 112)
[37] H.-K. Janssen and O. Stenull, *First-order phase transitions in outbreaks of co-infectious diseases and the extended general epidemic process*, Europhys. Lett., 113 (2016), art. 26005. (Cited on pp. 102, 103)
[38] J. O. Kephart and S. R. White, *Measuring and modeling computer virus prevalence*, in Proceedings of the IEEE Computer Society Symposium on Research in Security and Privacy, IEEE, 1993, pp. 2–15. (Cited on p. 92)
[39] W. O. Kermack and A. G. McKendrick, *A contribution to the mathematical theory of epidemics*, Proc. Roy. Soc. Lond. A Math. Phys. Engrg. Sci., 115 (1927), pp. 700–721. (Cited on p. 94)
[40] P. L. Krapivsky, S. Redner, and D. Volovik, *Reinforcement-driven spread of innovations and fads*, J. Statist. Mech. Theory Exp., 2011 (2011), art. P12003. (Cited on p. 95)

[41] C. J. Kuhlman and H. S. Mortveit, *Limit sets of generalized, multi-threshold networks*, J. Cellular Automata, 10 (2015), pp. 161–193. (Cited on pp. 96, 112)
[42] C. Kyriakopoulos, G. Grossmann, V. Wolf, and L. Bortolussi, *Lumping of degree-based mean-field and pair-approximation equations for multistate contact processes*, Phys. Rev. E, 97 (2018), art. 012301. (Cited on p. 95)
[43] J. Legrand, R. F. Grais, P.-Y. Boelle, A.-J. Valleron, and A. Flahault, *Understanding the dynamics of Ebola epidemics*, Epidemiology and Infection, 135 (2007), pp. 610–621. (Cited on p. 94)
[44] P. E. Lekone and B. F. Finkenstädt, *Statistical inference in a stochastic epidemic SEIR model with control intervention: Ebola as a case study*, Biometrics, 62 (2006), pp. 1170–1177. (Cited on pp. 93, 94)
[45] T. M. Liggett, *Interacting Particle Systems*, Springer, 1985. (Cited on pp. 92, 95)
[46] Y. Lin, J. C. Lui, K. Jung, and S. Lim, *Modelling multi-state diffusion process in complex networks: Theory and applications*, J. Complex Networks, 2 (2014), pp. 431–459. (Cited on p. 94)
[47] V. Marceau, P.-A. Noël, L. Hébert-Dufresne, A. Allard, and L. J. Dubé, *Adaptive networks: Coevolution of disease and topology*, Phys. Rev. E, 82 (2010), art. 036116. (Cited on p. 96)
[48] N. Masuda and N. Konno, *Multi-state epidemic processes on complex networks*, J. Theoret. Biol., 243 (2006), pp. 64–75. (Cited on p. 94)
[49] A. S. Mata and S. C. Ferreira, *Multiple transitions of the susceptible-infected-susceptible epidemic model on complex networks*, Phys. Rev. E, 91 (2015), art. 012816. (Cited on pp. 95, 104)
[50] A. Mellor, M. Mobilia, S. Redner, A. M. Rucklidge, and J. A. Ward, *Influence of Luddism on innovation diffusion*, Phys. Rev. E, 92 (2015), art. 012806. (Cited on p. 95)
[51] S. Melnik, J. A. Ward, J. P. Gleeson, and M. A. Porter, *Multi-stage complex contagions*, Chaos, 23 (2013), art. 013124. (Cited on pp. 96, 112)
[52] F. Morone and H. A. Makse, *Influence maximization in complex networks through optimal percolation*, Nature, 524 (2015), pp. 65–68. (Cited on p. 112)
[53] M. E. Newman, *Networks: An Introduction*, Oxford University Press, 2010. (Cited on pp. 92, 93, 96)
[54] T. W. Ng, G. Turinici, and A. Danchin, *A double epidemic model for the SARS propagation*, BMC Infectious Diseases, 3 (2003), p. 1. (Cited on p. 94)
[55] R. Pastor-Satorras, C. Castellano, P. Van Mieghem, and A. Vespignani, *Epidemic processes in complex networks*, Rev. Modern Phys., 87 (2015), pp. 925–979. (Cited on p. 94)
[56] R. Pastor-Satorras and A. Vespignani, *Epidemic spreading in scale-free networks*, Phys. Rev. Lett., 86 (2001), pp. 3200–3203. (Cited on p. 103)
[57] M. A. Porter and J. P. Gleeson, *Dynamical Systems on Networks: A Tutorial*, Springer, 2016. (Cited on p. 92)
[58] B. A. Prakash, D. Chakrabarti, N. C. Valler, M. Faloutsos, and C. Faloutsos, *Threshold conditions for arbitrary cascade models on arbitrary networks*, Knowledge Inform. Syst., 33 (2012), pp. 549–575. (Cited on p. 94)
[59] J. Sanz, C.-Y. Xia, S. Meloni, and Y. Moreno, *Dynamics of interacting diseases*, Phys. Rev. X, 4 (2014), art. 041005. (Cited on pp. 93, 95, 102, 103, 108)
[60] T. C. Schelling, *Dynamic models of segregation*, J. Math. Sociology, 1 (1971), pp. 143–186. (Cited on p. 95)
[61] M. Sellitto, D. De Martino, F. Caccioli, and J. J. Arenzon, *Dynamic facilitation picture of a higher-order glass singularity*, Phys. Rev. Lett., 105 (2010), art. 265704. (Cited on p. 110)
[62] B. Shulgin, L. Stone, and Z. Agur, *Pulse vaccination strategy in the SIR epidemic model*, Bull. Math. Biol., 60 (1998), pp. 1123–1148. (Cited on p. 94)
[63] M. Singer, *Introduction to Syndemics: A Critical Systems Approach to Public and Community Health*, John Wiley & Sons, 2009. (Cited on p. 108)
[64] M. Small and C. K. Tse, *Small world and scale free model of transmission of SARS*, Internat. J. Bifur. Chaos, 15 (2005), pp. 1745–1755. (Cited on p. 94)
[65] V. Sood and S. Redner, *Voter model on heterogeneous graphs*, Phys. Rev. Lett., 94 (2005), art. 178701. (Cited on p. 95)
[66] D. Stauffer and M. Sahimi, *Can a few fanatics influence the opinion of a large segment of a society?*, European Phys. J. B, 57 (2007), pp. 147–152. (Cited on p. 95)
[67] F. Vazquez, P. L. Krapivsky, and S. Redner, *Constrained opinion dynamics: Freezing and slow evolution*, J. Phys. A, 36 (2003), art. L61. (Cited on p. 95)

[68] F. Vazquez and S. Redner, *Ultimate fate of constrained voters*, J. Phys. A, 37 (2004), pp. 8479–8494. (Cited on p. 95)
[69] D. Volovik, M. Mobilia, and S. Redner, *Dynamics of strategic three-choice voting*, Europhys. Lett., 85 (2009), art. 48003. (Cited on p. 95)
[70] D. Volovik and S. Redner, *Dynamics of confident voting*, J. Statist. Mech. Theory Exp., 2012 (2012), art. P04003. (Cited on p. 95)
[71] D. J. Watts, *A simple model of global cascades on random networks*, Proc. Natl. Acad. Sci. USA, 99 (2002), pp. 5766–5771. (Cited on pp. 92, 96, 112)
[72] F. Xiong, Y. Liu, Z.-j. Zhang, J. Zhu, and Y. Zhang, *An information diffusion model based on retweeting mechanism for online social media*, Phys. Lett. A, 376 (2012), pp. 2103–2108. (Cited on p. 95)